International Journal for Housing Science and Its Applications
Publish August 10, 2025. Volume 46, Issue 4 Pages 968-980

https://doi.org/10.70517/ijhsa46490

A model for evaluating the impact of power fluctuation of optical storage and charging microgrids on the distribution network based on time series data

Qingsheng Li[1], Jian Wang[2], Zhen Li[1,*], Linbo Wang[2] and Zhanpeng Xu[3]
[1] Power Grid Planning Research Center of Guizhou Power Grid Co., Ltd., Guizhou, Guiyang, 710068, China
[2] Guizhou Grid Co., Ltd. Guiyang Power Supply Bureau, Guizhou, Guiyang, 710068, China
[3] China Energy Engineering Group Guangdong Electric Power Design Institute Co., Ltd., Guangzhou, Guangdong, 510663, China
Corresponding authors: (e-mail: 18300877542@163.com).

Abstract As an emerging power system form, the power output characteristics of optical storage-charging integrated microgrids are characterized by significant intermittency and stochasticity, which bring new challenges to the safe and stable operation of distribution grids. Aiming at the problem of evaluating the impact of power fluctuation of optical storage-charging microgrids on the reliability of distribution grids, this paper constructs a full-time simulation and analysis model based on time series data and a hybrid CNN-GRU neural network prediction model. By analyzing different fault scenarios, a microgrid reliability assessment index system is established, and the method of extracting spatial features by convolutional neural network and capturing timing features by gated recurrent unit is applied to realize accurate prediction of PV power. The case analysis based on the IEEE RBTS test system shows that the SAIFI index of the distribution system decreases from 1.6354 to 1.4795 after microgrid access, and the power supply availability rate increases from 0.99936 to 0.99947, which significantly improves the system reliability. The prediction accuracies of the CNN-GRU model are better than those of the traditional methods in all four seasons, and the NMAI indexes of the CNN-GRU model are better than those of the traditional methods, and the NMAI indexes are better than the traditional methods in all four seasons. Attention model with a maximum reduction of 59.2% in NMAE metrics and 45.4% in NRMSE metrics. The results verify the effectiveness of the proposed model in microgrid output fluctuation assessment and prediction, and provide theoretical support for distribution network planning and operation.

Index Terms Time series data, optical storage charging microgrid, output fluctuation, distribution grid, CNN-GRU, reliability assessment

I. Introduction

In recent years, in order to promote the reduction of carbon emissions and realize green development, electric vehicles have been favored and supported by more users for their clean and almost zero-emission advantages [1]. As a new type of load, the charging load of electric vehicles is mainly influenced by the user's life habits with great randomness [2]. On the one hand, most of them are highly dependent on external power supply and cannot realize independent power supply; on the other hand, there is a lack of stable internal energy storage equipment, which makes it impossible to regulate energy flexibly [3]-[5]. Meanwhile, due to the proliferation of electric vehicles, a large number of electric vehicles charging into the grid will lead to an increase in the peak-valley difference of the grid, further aggravating the burden of the safe operation of the power system [6], [7]. Therefore, combining PV systems, energy storage systems and charging piles can effectively utilize their respective advantages to obtain better economic and environmental benefits [8], [9].

The complementary nature of PV systems and energy storage systems in microgrids can give full play to their respective strengths, both through PV power generation to electric vehicles and other loads direct power supply to realize the local consumption of PV energy and reduce the impact of electric vehicle charging on the power system [10]-[13]. At the same time, the energy storage system can effectively alleviate the uncertainty of PV output and improve the utilization rate of PV power, store part of the electrical energy when the PV power generation is large, and supply power to electric vehicles and other loads when the PV power generation is insufficient [14]-[16]. However, considering that the grid integration of large-scale renewable energy generation can adversely affect the normal operation of the power system, it is necessary to evaluate the power output fluctuation of the photovoltaic storage-charged microgrid in order to formulate an optimal scheduling strategy for the microgrid [17]-[20].

This study proposes a method for assessing the impact of power output fluctuation of optical storage-charged microgrids on distribution grids based on time series data. Firstly, a full-time sequence simulation model containing the microgrid distribution system is established, and by analyzing the response characteristics of the system under different fault scenarios, an assessment index system is constructed with comprehensive consideration of reliability and economy. Then, the key factors affecting PV power are analyzed in depth, including seasonality, radiation intensity, temperature and humidity and other environmental parameters, and a CNN-GRU hybrid neural network model is constructed to realize the accurate prediction of PV power, which provides data support for the assessment of power fluctuation of microgrid.

II. Reliability assessment model for microgrid-containing distribution networks based on time series data

In this chapter, based on the time series data, the reliability assessment of the distribution network containing the optical storage and charging microgrid is carried out through full time series simulation analysis with reliability indexes, and the economic modeling of the optical storage and charging microgrid is realized.

II. A.Full-time sequence simulation and analysis method for optical storage charging microgrids

For microgrids, the reliability of the system is more susceptible to the disturbance of the DG output characteristics, the reliability of the components, the operation mode of the ESS and the load timing fluctuations. In this paper, the failure of MT, PV, and ESS in one and only one component is called the first-order fault, taking into account the first-order faults of DG and ESS, and assuming that the lines and transformers can work normally, and whether they fail or not does not affect the reliability of the system, the state of the components and load curtailment or not at each time period are classified by the full-time sequence simulation method. The scenarios are classified. Where $P_{\mathrm{DG}}(h)$ is the total MT and PV output power.

(1) Scenario 1: MT, PV and ESS are all fault-free. At this time, ESS flexibly changes the operation mode according to the possible power deficit between $P_{\mathrm{DG}}(h)$ and the total power of the load to maintain the system balance, if there is still a power deficit after ESS is fully discharged, then the load is cut $P_{shedding}^{L}(h)=P_{L}(h)-P_{DG}(h)-P_{dch}^{\max}(h)$.

(2) Scenario 2: MT fails, PV and ESS are normal. At this time, the microgrid is prioritized by the PV, ESS discharges to make up for the shortfall, and if there is still a power deficit after ESS discharges completely, the load is cut at this time $P_{shedding}^{L}(h)=P_{L}(h)-P_{PV}(h)-P_{dch}^{\max}(h)$.

(3) Scenario 3: PV is in fault state or intermittent period, MT and ESS are normal. At this time, the system power is supplied by MT, and the shortfall is made up by ESS discharge. If there is still a power shortfall after ESS discharge, the load is cut $P_{shedding}^{L}(h)=P_{L}(h)-P_{MT}(h)-P_{dch}^{\max}(h)$.

(4) Scenario 4: ESS fails, MT and PV are normal. Due to the randomness of PV output power and the lack of energy caching device to suppress its output, it is necessary to cut the load power equal to the PV output to maintain the system balance, at this time, the microgrid is still supplied by the MT, and the cut load $P_{shedding}^{L}(h)=P_{L}(h)-P_{DG}(h)$.

II. B.Reliability Assessment Metrics and Processes for Distribution Grids with Microgrids

II. B. 1) Reliability indicators

Reliability of power supply is a primary consideration in the capacity planning of distribution networks containing microgrids. For this reason, reliability indicators that intuitively reflect the demand of various types of load users and sensitively characterize the changes in the capacity and power of microgrids should be selected. The probabilistic indicators selected in this paper include Loss of Load Probability (LOLP), Average Supply Availability Indicator (ASAI), Frequency and Duration Indicators, including System Average Outage Duration Indicator (SAIDI), Customer Average Outage Duration Indicator (CAIDI), System Average Frequency of Outages Indicator (SAIFI), and Electricity Shortage Indicator (ENS). Upon convergence comparison, the indicator CAIDI converges significantly slower than the other indicators. After setting, the variance coefficient of CAIDI is less than 0.016 as the sampling termination condition, and the calculation of the variance coefficient is shown in equation (1):

$$\beta_{CAIDI}=\frac{\sqrt{\frac{V_{CAIDI}}{H}}}{E_{CAIDI}} \tag{1}$$

where, β_{CAIDI}, V_{CAIDI}, E_{CAIDI} are the coefficient of variance, variance, and expectation of CAIDI, respectively, and H is the simulation length.

In this paper, the variance coefficient of the indicator with the slowest convergence rate is used as the reference for sampling termination. After the convergence test, with 8 years as the simulation length and a sampling interval of 1h, the sampling termination condition is met.

II. B. 2) Reliability assessment process

In this paper, we carry out a full-time simulation reliability assessment of distribution networks containing microgrids, which consists of the following basic steps:

(1) Initialize the data and set the simulation time.

(2) According to the failure rate of each component, find out the failure-free time $T_{TTF,i}$ of component i, and take the minimum value of $T_{TTF,i}$ as the system uptime, and accumulate it into the total simulation time.

(3) Find the component i repair time $T_{TTR,i}$ based on the repair rate of each component.

(4) Based on the $T_{TTF,i}$ and $T_{TTR,i}$ of the components, calculate the operating state sequence of all components during the total simulation time.

(5) Based on the state sequences of the components, the state sequences of the system are obtained and accumulated to get the reliability index value of the system.

II. C.Economic modeling of optical storage charging microgrids

II. C. 1) Objective function

Based on the completion of the preparatory work for the system reliability assessment, the microgrid total cost minimization function model shown in Eq. (2) is established to seek the optimal configuration of DG and ESS:

$$\min C = C_{MT} + C_{PV} + C_{ESS} \tag{2}$$

where, C_{MT}, C_{PV} and C_{ESS} are the MT yearly cost, PV yearly cost and ESS full life cycle cost respectively.

(1) The MT and PV annual cost functions are:

$$C_{MT} = \left[\alpha_{MT} \frac{r_0(1+r_0)^{y_{MT}}}{(1+r_0)^{y_{MT}} - 1} + \mu_{MT} \right] N_{MT} \tag{3}$$

$$C_{PV} = \left[\alpha_{PV} \frac{r_0(1+r_0)^{y_{PV}}}{(1+r_0)^{y_{PV}} - 1} + \mu_{PV} \right] N_{PV} \tag{4}$$

where α_{MT} and α_{PV} are the MT and PV construction costs, respectively. r_0 is the discount rate. y_{MT} and y_{PV} are the MT and PV operating years, respectively. μ_{MT} and μ_{PV} are the MT and PV annual operation and maintenance costs, respectively. N_{MT} and N_{PV} are the number of MT and PV units, respectively.

(2) The ESS full life cycle cost function is:

$$\begin{cases} C_{ESS} = C_{CC} + C_{OC} \\ C_{CC} = (C_{E,ESS} E_{ESS}(h) + C_{P,ESS} P_{ESS}(h)) \cdot \dfrac{r_0(1+r_0)^{y_{ESS}}}{(1+r_0)^{y_{ESS}} - 1} \\ C_{OC} = (C_{E,ESS} E_{ESS}(h) + C_{P,ESS} P_{ESS}(h))\lambda \end{cases} \tag{5}$$

where, C_{CC} and C_{OC} are the ESS one-time construction cost and O&M cost, respectively. $C_{E,ESS}$ and $C_{P,ESS}$ are the ESS unit capacity cost and unit power cost, respectively. y_{ESS} is the ESS operating life. λ is the ratio of O&M cost to initial investment cost for ESS operation to the target year.

II. C. 2) Constraints

The constraints containing ESS charging and discharging power, ESS state of charge (SOC) and system power balance are written according to the objective function setting:

$$\begin{cases} S_{SOC}^{\min} \le S_{SOC}(h) \le S_{SOC}^{\max} \\ P_L(h) = P_{PV}(h) + P_{MT}(h) + P_{ESS}(h) \\ -P_{dch}^{\max}(h) \le P_{ESS}(h) \le P_{ch}^{\max}(h) \end{cases} \tag{6}$$

where, $S_{SOC}^{\max}$ and $S_{SOC}^{\min}$ are the upper and lower SOC tolerance limits, respectively.

II. D.Analysis of examples

II. D. 1) Basic data

An arithmetic case analysis is performed on the IEEE RBTS test system with the IEEE RBTS Bus6-F4 feeder, and the microgrid power supply area is shown in Figure 1.

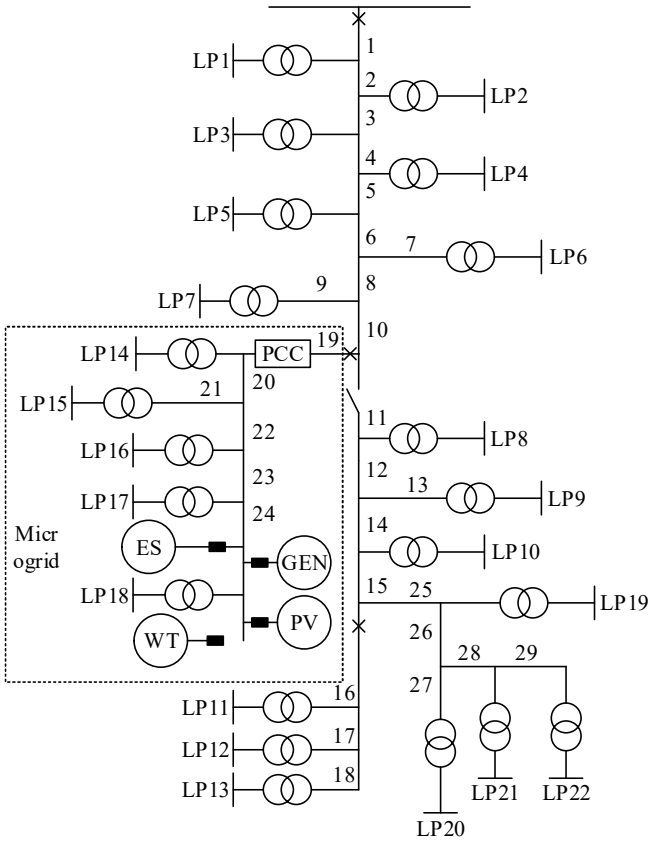

Figure 1: Improved IEEE RBTS Bus6-F4 system

The system has 22 load points, 22 distribution transformers, 29 lines, 3 circuit breakers, one sectionalized switch and 576 users, and the load parameters and equipment reliability parameters and feeder segment data are shown in Tables 1 to 3. The microgrid islanding operation mode switching success probability is set to 0.88, the microgrid internal load cut sequence is LP14-LP18 in order, and the microgrid scenery natural resources are adopted from the data of a region in central China.

Table 1: Load data

Load point serial number	Peak load /kW	Number of users /households	Load point serial number	Peak load /kW	Number of users /households
2	331.8	128	7	804.7	2
5	376.5	130	9,21	748.2	2
1,6	304.6	150	3,13,17	660.8	2
15,20	511.2	2	10,12,16,22	291.4	78
4,18	692.3	2	8,11,14,19	285.9	80

Table 2: Reliability parameters of the equipment

Name	Failure rate	Average repair time /h
Line	0.04 times/ (km · year)	3.5
Distribution transformer	0.012 times/ (Taiwan · year)	28
Switch	0.005 times per year	5

Table 3: Feeder section data

Feeder type	Length /km	Feeder section serial number
1	0.5	7,13
2	0.65	27
3	0.7	9,21
4	0.8	4,10
5	1.7	3,5,8,15,20,28
6	2.4	2,6,18,23,26
7	2.7	1,12,16,22,15
8	3.3	11,17,19,24,19
9	3.6	14

Three scenarios are set up in this chapter, Scenario 1 without microgrids and Scenarios 2 and 3 containing microgrids with different power configuration capacities. By comparing the three scenarios, the impact of microgrid access on the reliability of the distribution network can be quantitatively analyzed. The specific configuration scheme of microgrid capacity is shown in Table 4.

Table 4: Microgrid capacity configuration scheme

	Wind power capacity /MW	Photovoltaic capacity /MW	Battery capacity /MW
Scheme 1	0	0	0
Scheme 2	2	2.5	9
Scheme 3	1.5	2	9

II. D. 2) Calculation results of reliability indicators

The load point reliability indicators under the three scenarios are shown in Fig. 2, where (a) and (b) denote the fault rate and average annual outage time, respectively. It can be seen that the reliability indexes of the load points within the microgrid have improved significantly, the average annual failure rate and average annual outage time have decreased significantly, and the improvement of the reliability of important load points is especially obvious. Since this paper does not take into account the external power supply of the microgrid, it is not possible to see the impact of the microgrid on the reliability of power supply to its external load points. Comparing the different capacity allocation schemes, it can be seen that increasing the allocated capacity of distributed power sources can help improve the reliability of power supply at load points. However, microgrid capacity allocation not only needs to consider the reliability, but also needs to consider the economy, environmental protection and other indicators, microgrid capacity optimization is a very important aspect of microgrid planning and design.

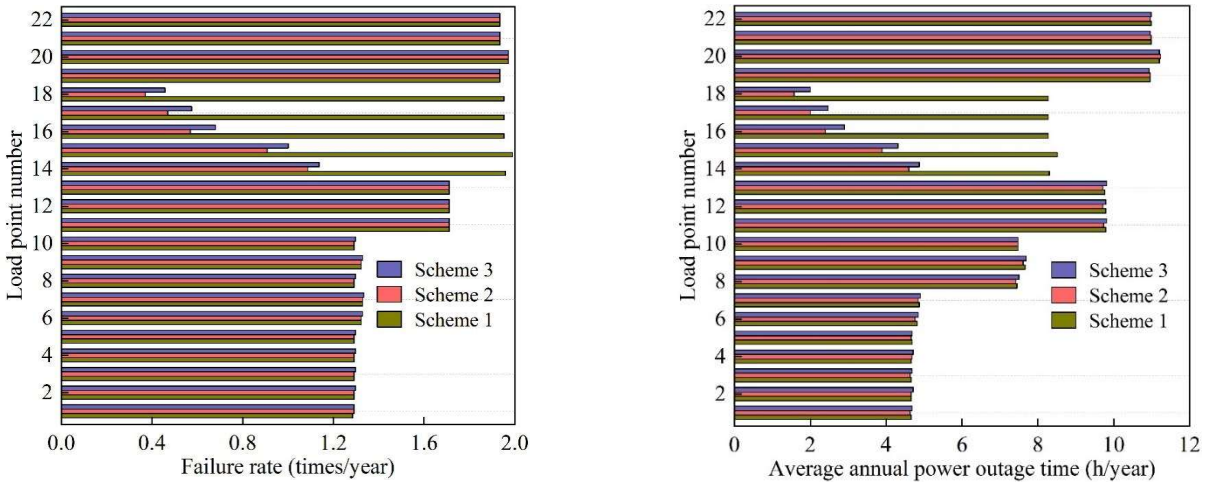

(a) Failure rate (b) Average annual power outage time

Figure 2: Reliability indicators of load points before and after microgrid access

The reliability indicators for the distribution system under different configuration scenarios are shown in Table 5, where there is no microgrid access in scenario 1. From the data in the table, it can be seen that microgrid access improves the power supply reliability of the distribution system, which is due to the fact that the microgrid has a certain probability to turn into island operation when the distribution network components fail, ensuring the continuous and stable power supply of loads in the microgrid, especially the important loads. Comparison of the calculation results of Scenario 2 and Scenario 3 shows that increasing the distributed power configuration of the microgrid can improve the reliability of the system, but the increase in the configuration capacity affects the economy of the system, so the power capacity of the microgrid should be optimally configured according to the actual situation.

Table 5: Reliability indicators of the power distribution system

	SAIFI (times/user · year)	SAIDI (h/ user · year)	ENS (MW ·h/ year)	ASAI
Scheme 1	1.6354	6.5274	35.62	0.99936
Scheme 2	1.4795	5.8789	30.15	0.99947
Scheme 3	1.44961	6.0147	30.79	0.99942

The reliability indicators of the microgrid system under different configuration schemes are shown in Table 6. Comparing the reliability indexes of the whole distribution system, it can be seen that the improvement of the power supply reliability indexes of the microgrid system is obvious, indicating that the microgrid has a significant effect in improving the power supply reliability of its internal loads. Comparing different configuration schemes, it can be seen that increasing distributed power capacity allocation is conducive to improving the reliability of the microgrid system.

Table 6: Reliability indicators of microgrids under different configuration schemes

	SAIFI (times/user · year)	SAIDI (h/ user · year)	ENS (MW ·h/ year)	ASAI
Scheme 2	0.8247	3.2583	2.52	0.99975
Scheme 3	0.9074	3.5749	2.97	0.99971

III. CNN-GRU based power fluctuation prediction for optical storage and charging microgrids

In order to further assess the impact of photovoltaic storage-charged microgrid power fluctuations on the distribution network, this chapter analyzes the influencing factors of photovoltaic (PV) power and realizes an accurate prediction of short-term PV power, i.e., power fluctuations, in microgrids by using a hybrid CNN-GRU neural network model.

III. A. Analysis of factors affecting the power of photovoltaic power generation

In order to find the effect of meteorological environmental factors on PV power generation, in this section, a laboratory 15kWp vegetative PV power generation system will be analyzed in conjunction with the NWP data during the same observation time in the region, and the main environmental factors to be investigated include seasonal factors, radiation intensity factors, temperature factors, and humidity factors.

(1) Influence of seasonal factors on PV power generation

The power output curves of the PV power generation system on a typical day in four seasons are shown in Fig. 3. It can be seen that different seasons have different sunrise and sunset times, which affects the length of the daily PV power generation time: summer sunrise is earlier and sunset is later, and the PV power generation time is longer in a day. In winter, the sunrise time is late and the sunset time is early, and the PV power generation time is shorter in a day. At the same time, because the PV power is affected by the temperature, the daily power generation in winter is reduced compared with other seasons.

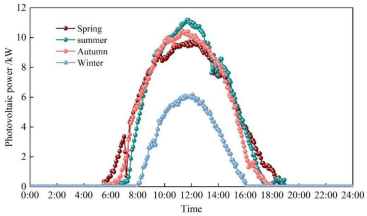

Figure 3: Photovoltaic power curves on typical days in four seasons

(2) Influence of meteorological conditions on photovoltaic power generation

Photovoltaic power curve in different seasons has different characteristics, from the perspective of energy conversion, photovoltaic power generation energy from solar radiation energy, but also by the environmental temperature, humidity and other meteorological conditions. In this section, solar radiation intensity, temperature and humidity are taken as several important meteorological condition influences affecting PV output power, and the relationship between each influence factor and PV output power is analyzed by graphing method. In order to facilitate the comparison, all data are normalized as shown in equation (7):

$$M_i = \frac{x_i - x_{\min}}{x_{\max} - x_{\min}} \left(i = 1, 2, \ldots, n\right) \tag{7}$$

M_i and x_i denote the normalized and actual values, respectively, and $x_{\min}$ and $x_{\max}$ denote the minimum and maximum values in the data set, respectively.

The PV power curve and the total radiation intensity curve are shown in Fig. 4. It can be seen that there is a strong consistency between the PV power curve and the radiation intensity curve, which indicates that the PV power and the solar radiation intensity have certain correlation characteristics. However, in some moments, the solar radiation intensity may be consistently high but the PV output power does not increase consistently, this is because in addition to the radiation intensity affects the PV power, there are other factors affecting the PV output power.

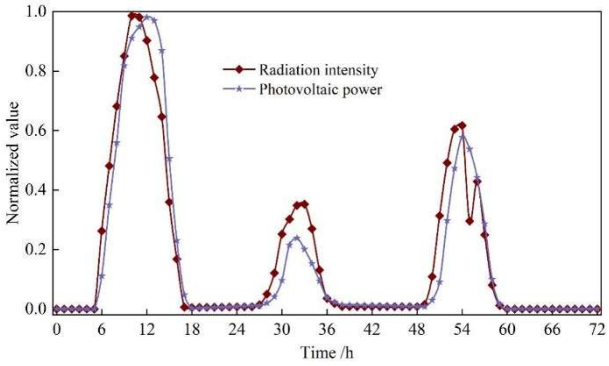

Figure 4: Relationship between photovoltaic power and radiation intensity

For cloudy and rainy weather, due to cloud cover, part of the solar radiation by the scattering effect of clouds become scattered radiation, the total solar radiation Q is equal to the scattering radiation D and direct radiation S' sum, when the cloudy and rainy weather, more clouds, direct radiation is small, more scattered radiation, direct radiation and scattered radiation is smaller, the daily power generation is less, sunny days with good sunshine conditions is the opposite. In this paper, the ratio of solar scattered radiation D to direct radiation S' is the radiation scattering ratio R. From the above theory, the PV power fluctuation index K = daily power generation / radiation scattering ratio is defined.

In order to specify the relationship between the radiation scattering direct ratio and daily power generation, using statistical methods, the laboratory 15kWp photovoltaic power generation system August 5, 2022 - August 30, 2022 normal operation day PV daily power generation effective data collected with the day of the radiation scattering direct ratio and fluctuation index K, to get the photovoltaic power fluctuation index shown in Table 7.

It can be seen that the daily power generation basically decreases with the increase of the radiation scattering direct ratio. When the daily power generation is larger, the reason is that the weather conditions are better on that day and the PV power curve is smoother. When the daily power generation is small, the reason is that the weather conditions on that day are poor, mostly cloudy and rainy, and the fluctuation of the PV power curve is more violent. According to the fluctuation index K and the corresponding actual PV power fluctuations, its characteristics can be summarized as follows: when K>160 for PV fluctuations smaller, 40<K<160 PV power fluctuations are more intense, K<40 PV power fluctuations are intense.

Table 7: Photovoltaic power generation power fluctuation index

Date	5	6	7	8	9	10	11	12	13	14	15	16	17
Daily power generation (Kw·h)	58.21	64.94	64.93	47.26	61.57	30.95	73.42	60.84	53.42	49.73	75.86	64.98	47.55
Radiation diffusion-direct ratio (D/S')	0.526	0.514	0.632	1.745	0.863	3.694	0.385	1.678	1.975	1.273	0.281	0.574	2.042
Volatility index K	110.7	126.3	102.7	27.1	71.3	8.4	190.7	36.3	27.0	39.1	270.0	113.2	23.3
Date	18	19	20	21	22	23	24	25	26	27	28	29	30
Daily power generation (Kw·h)	36.84	40.32	63.75	65.41	51.46	57.42	58.63	21.81	50.27	68.43	66.59	57.82	54.91
Radiation diffusion-direct ratio (D/S')	6.044	28.745	1.641	1.053	2.432	1.964	1.653	200.415	5.624	0.307	0.526	0.910	1.908
Volatility index K	6.1	1.4	38.8	62.1	21.2	29.2	35.5	0.11	8.94	222.9	126.6	63.5	28.8

The PV power and temperature relationship curve is shown in Fig. 5. It can be seen that the atmospheric temperature and the PV output power have a similar trend, the PV output power increases the temperature also rises, the PV power decreases the temperature also decreases, which shows that the PV power and the atmospheric temperature has a certain positive correlation.

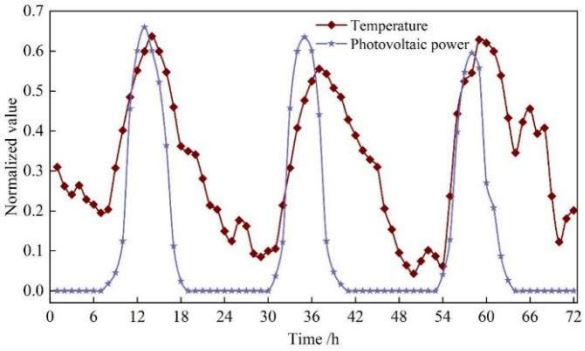

Figure 5: Relationship between PV power Generation capacity and temperature

The PV power versus relative humidity curve is shown in Fig. 6. It can be observed that the relationship between relative humidity and PV power in a day shows an opposite trend, i.e., the valley region of the humidity curve corresponds to the peak region of PV power, which is due to the fact that the time tends to midday when the solar radiation is enhanced and the atmospheric relative humidity decreases and the PV power increases. This is because the time tends to evening when solar radiation decreases and atmospheric humidity increases the PV power decreases, which indicates that the relative humidity also has a strong correlation with the PV output power.

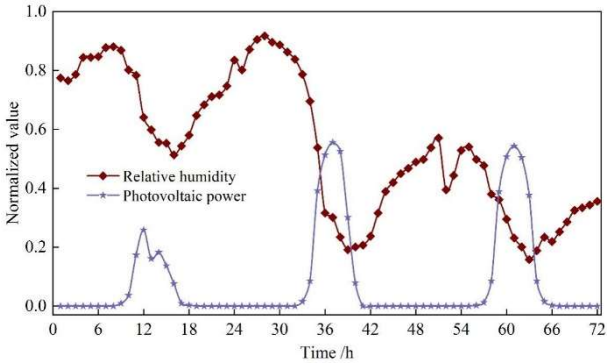

Figure 6: The relationship between PV power generation capacity and air relative humidity

III. B. Short-term PV power prediction model based on CNN-GRU

In order to improve the prediction accuracy of photovoltaic (PV) power in light-storage-charged microgrids, a short-term PV power prediction model based on a hybrid CNN-GRU neural network is constructed in this chapter.

III. B. 1) Convolutional Neural Networks

Convolutional Neural Network (CNN) [21] is a deep learning algorithm often used for image, text and signal inputs and consists of a stack of layers for extracting features of an object. CNN consists of an input layer, a convolutional layer, a pooling layer, a fully connected layer, and an output layer. Convolutional layer is the key to efficient feature extraction in CNN, in this paper convolutional layer is mainly applied to feature extraction of PV power related data.

(1) Input layer: the input layer mainly receives data related to PV power plant, such as meteorological information irradiance, temperature, etc. and historical power data. And the input data are preprocessed, including de-mean and normalization.

(2) Convolutional layer: the convolutional layer is mainly used to extract features from the input data. The convolution operation extracts high-level features from the input data by sliding the convolution kernel over the input data, and the local information is convolved with the convolution kernel, and the convolution operation process is shown in equation (8):

$$M_j = f\left(\sum M_{j-1} \otimes W_j + b_j\right) \tag{8}$$

where M_j is the input characteristic of the j th layer, $f(x)$ is the activation function, $\otimes$ is the convolution operation, W_j is the weight of the convolution kernel of the j th layer, and b_j is the threshold.

(3) Pooling Layer: The main role of the pooling layer is to compress the data and reduce the computational complexity while maintaining important information. The most common pooling operation is maximum pooling, which selects the maximum value in each pooling window as a representative. The pooling layer helps to improve the translational invariance of the model and reduce overfitting.

(4) Fully Connected Layers: the main role of fully connected layers is to map high-level features from the convolution and pooling layers to the output of the network. These layers contain multiple neurons, each connected to all neurons in the previous layer. The fully connected layers generate the final features for representation by learning the weights and biases.

(5) Output Layer: the main role of the output layer is to output the result of the CNN network.

The core of CNN lies in the use of local sensing and parameter sharing mechanism. This unique design effectively reduces the complexity of model parameters, which in turn significantly improves the training speed and efficiency of the network.

III. B. 2) Door-controlled circulation units

Gated Recurrent Unit (GRU) [22] is a variant of Long Short-Term Memory (LSTM) networks, which is widely used in academia. GRU uses reset gates and update gates to overcome the long term dependency problem and combines the data units and hidden layer states to solve the gradient vanishing problem. Compared to LSTM, GRU networks contain only two gate structures, reducing the number of training parameters. This makes the GRU network easier to converge and alleviates the overfitting problem of the LSTM network, while maintaining the excellent performance of the LSTM network in prediction tasks. The specific formulation of the GRU network is shown below:

$$\begin{cases} r_t = \sigma\left(W_r \times \left[h_{t-1}, x_t\right]\right) \\ z_t = \sigma\left(W_z \times \left[h_{t-1}, x_t\right]\right) \\ \tilde{h}_t = \tanh\left(W \times \left[r_t * h_{t-1}, x_t\right]\right) \\ h_t = \left(1 - z_t\right) * h_{t-1} + z_t * \tilde{h}_t \end{cases} \tag{9}$$

where z_t denotes the update gate, which is mainly used for forgetting and remembering. r_t is the reset gate, which is used to determine whether or not to merge the current state with previous information. $\tilde{h}_t$ denotes an intermediate memory state. W_z and W_r are the connection weights of the update and reset gates, respectively. σ and $\tanh$ are activation functions.

III. B. 3) CNN-GRU hybrid neural network models

The hybrid CNN-GRU structure proposed in this chapter is shown in Fig. 7. In the proposed structure, CNNs are used for features to perform sequence representation and then effective sequence learning is performed using multilayer GRUs.The CNN layers are used to extract spatial features from the input fine data and then feed them into the multilayer GRUs.In this chapter, two CNN layers with Relu activation function and kernel size 2 are used, and the filters of the first and the second layers are 1 × 16 and 1 × 8, respectively .After extracting the spatial features, they are fed into the GRU layer. Two GRU layers are used to model the temporal features and finally the predicted values are output through the fully connected layers.

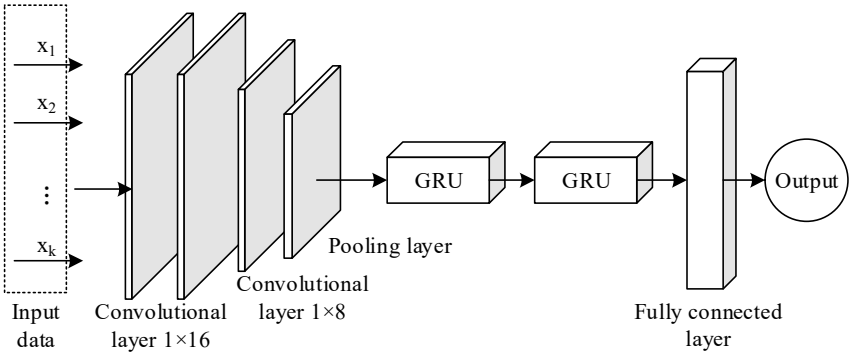

Figure 7: CNN-GRU network Structure

In PV power prediction, spatial features are extracted by CNN network and then temporal features are extracted by GRU network, which can take into account the hidden information and obtain better prediction results.

III. C. PV Power Prediction and Result Analysis

Multiple models are selected for comparative analysis to verify the advantages of the prediction model proposed in this paper, and the models involved in the comparison are LSTM, LSTM-Attention and GRU, respectively. one day in each of the four seasons is randomly selected for the prediction of PV power generation, and the prediction curves are obtained and compared with the actual data, and the comparison of the prediction results of different seasons is shown in Fig. 8, and the results of the comparison of the different seasons are shown in Fig. 8, and the results of the comparison of the different seasons are shown in Fig. 8, and the results of the comparison of the different seasons are shown in Figs. 8, (a) ~ (d) The comparison results of different seasons are shown in Fig. 8, (a)~(d), which represent the comparison results of four seasons, namely, spring, summer, fall and winter, respectively.

It can be visualized from the prediction curve: in spring, the fluctuation of PV power is not obvious, and the PV power will drop suddenly in a few periods due to cloud cover and other circumstances. In summer, with sufficient light and good weather conditions, the power fluctuation is almost non-existent and the PV power is the highest in the year. In the fall, the PV power fluctuates more, the accuracy of the prediction results decreases, and the PV power is higher. Compared to other seasons, in winter, there is a significant decrease in PV power and the power generation period is narrowed.

By training the model for different seasons, the purple line indicating the prediction results of the CNN-GRU PV power generation prediction model proposed in this paper is the most overlapped with the dark cyan line indicating the actual PV power in all four seasons. It can also be seen that the combined model overlaps with the actual values better than the single model, and the LSTM prediction curve overlaps with the actual value curve better than the GRU.

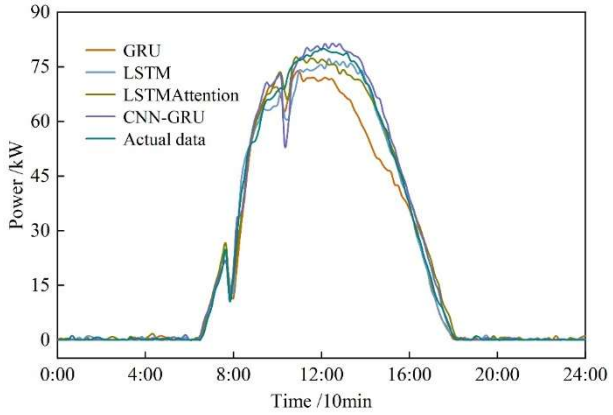

(a) Spring

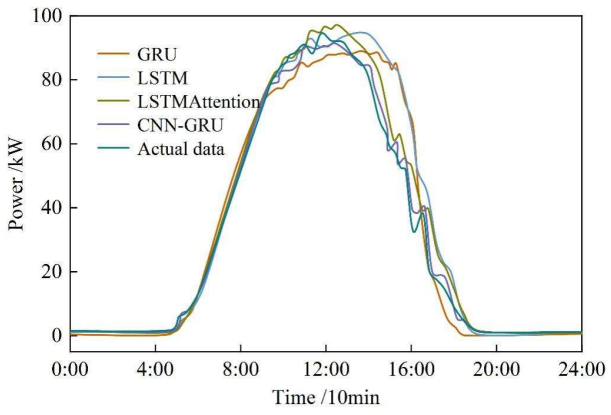

(b) Summer

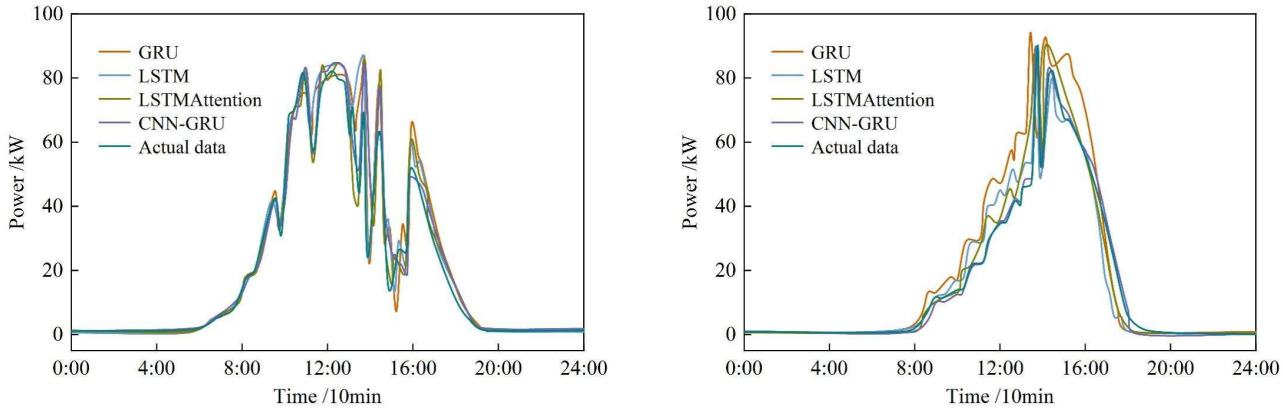

(c) Autumn (d) Winter

Figure 8: Comparison of prediction results in different seasons

The comparison of performance evaluation indexes of PV power prediction model is shown in Table 8. In order to eliminate the influence of data magnitude on the evaluation value, this paper uses the normalized evaluation indexes of mean absolute error (NMAE), root mean square error (NRMSE) and coefficient of determination (NR^2), and the smaller the values of NMAE and NRMSE indexes, the better, and the larger the value of NR^2 indexes, the better. In the table, A, B, C and D represent the datasets for the four seasons of spring, summer, fall and winter, respectively.

It can be seen that the prediction accuracy of the models GRU and LSTM is poor, the accuracy of LSTM-Attention is improved due to the addition of the attention mechanism, and the CNN-GRU model proposed in this paper has the best prediction effect. Compared with the LSTM-Attention model, the NMAE of this paper's model in the four seasons is reduced by 59.2%, 54.5%, 38.4%, and 49.6%, and the NRMSE is reduced by 45.4%, 35.2%, 33.3%, and 34.7%, respectively.

The training datasets of different seasons also have an impact on the prediction accuracy of the model, and the model is trained on summer dataset B. Due to the abundant light and better climatic conditions, the resulting predictions are more accurate compared to other seasons. Under the training of fall dataset C, the prediction accuracy decreases compared to other seasons due to the large fluctuation of PV power and environmental factors, and the NMAE and NRMSE in the proposed model in this paper are reduced by 64.4% and 50.4% in summer compared to fall, respectively.

Table 8: Comparison of performance evaluation indicators for prediction models

Method	Evaluation index	A	B	C	D
CNN-GRU	NMAE	0.0089	0.0080	0.0225	0.0131
	NRMSE	0.0208	0.0197	0.0397	0.0271
	NR^2	0.9923	0.9944	0.9798	0.9901
LSTM-Attention	NMAE	0.0218	0.0176	0.0365	0.0260
	NRMSE	0.0381	0.0304	0.0595	0.0415
	NR^2	0.9818	0.9857	0.9553	0.9758
LSTM	NMAE	0.0403	0.0376	0.0481	0.0445
	NRMSE	0.0726	0.0610	0.0908	0.0834
	NR^2	0.9519	0.9553	0.9394	0.9476
GRU	NMAE	0.0398	0.0382	0.0540	0.0463
	NRMSE	0.0705	0.0652	0.1034	0.0877
	NR^2	0.9529	0.954	0.9294	0.9411

IV. Conclusion

The access of the photovoltaic storage-charged microgrid significantly improves the power supply reliability of the distribution system, and the IEEE RBTS test system verifies that the distribution system containing the microgrid has significant improvement in several reliability indicators compared with the traditional system. The improvement in reliability indicators at the load points within the microgrid is particularly prominent, with the system average outage duration indicator decreasing from 6.5274 hours to 5.8789 hours, and the power deficit indicator decreasing from 35.62 MWh to 30.15 MWh. Through in-depth analysis of the factors affecting PV power, it is found that meteorological conditions such as seasonality, radiation intensity, temperature and humidity have a significant impact on PV power, and the established model of the relationship between the radiation scattering ratio and daily power generation is able to effectively quantify the fluctuation characteristics of PV power. The CNN-GRU hybrid neural network model performs excellently in the prediction of PV power, and it has obvious advantages compared with a single model, especially under the conditions of sufficient light in summer, the prediction accuracy of CNN-GRU is very high. The established model not only accurately evaluates the impact of photovoltaic power fluctuations on the distribution grid, but also provides a scientific basis for the optimal allocation of microgrid capacity and the formulation of operation strategies, which is of great significance for promoting the scale application of distributed energy resources.

Funding

This work was supported by China Southern Power Grid Company Technology Project (GZKJXM20240013).

References

[1] Moriarty, P., & Wang, S. J. (2017). Can electric vehicles deliver energy and carbon reductions?. Energy Procedia, 105, 2983-2988.
[2] Xia, X., Li, P., Xia, Z., Wu, R., & Cheng, Y. (2022). Life cycle carbon footprint of electric vehicles in different countries: A review. Separation and Purification Technology, 301, 122063.
[3] Avci, B., Girotra, K., & Netessine, S. (2015). Electric vehicles with a battery switching station: Adoption and environmental impact. Management Science, 61(4), 772-794.
[4] Wu, H. (2021). A survey of battery swapping stations for electric vehicles: Operation modes and decision scenarios. IEEE Transactions on Intelligent Transportation Systems, 23(8), 10163-10185.
[5] Ahmad, F., Saad Alam, M., Saad Alsaidan, I., & Shariff, S. M. (2020). Battery swapping station for electric vehicles: opportunities and challenges. IET Smart Grid, 3(3), 280-286.
[6] Sun, X. H., Yamamoto, T., & Morikawa, T. (2016). Fast-charging station choice behavior among battery electric vehicle users. Transportation Research Part D: Transport and Environment, 46, 26-39.
[7] Koirala, K., & Tamang, M. (2022). Planning and establishment of battery swapping station-A support for faster electric vehicle adoption. Journal of Energy Storage, 51, 104351.
[8] Zhu, Z. B., Sun, S. M., Ding, Y. M., & Huang, S. P. (2023). Research on control strategy of hybrid energy storage system with optical storage microgrid. Journal of Electrical Engineering & Technology, 18(4), 2835-2845.
[9] Yu, C., Yang, L., Zhang, S., Liu, J., Wan, J., & Song, M. (2024, November). Research on capacity configuration method of optical storage charging integrated charging station considering economic and environmental benefits. In Journal of Physics: Conference Series (Vol. 2896, No. 1, p. 012045). IOP Publishing.
[10] Wang, R., Wu, Z., & Sun, Z. (2024). Optimization of charging-station location and capacity determination based on optical storage, charging integration, and multi-strategy fusion. J. Green Econ. Low-Carbon Dev, 3(1), 1-14.
[11] Tianqi, L., Jing, G., Heyan, Z., & Guochen, Y. (2023). Optimization of hybrid energy storage based on micro grid optical storage and DC in certain regions. International Journal of Frontiers in Engineering Technology, 5(1).
[12] Li, Y., Zhang, X., Qi, C., Qu, Y., Ling, A., Sun, X., & Zhang, J. (2024, August). Modeling and Design of Photovoltaic Storage and Charging DC Microgrid System. In 2024 3rd International Conference on Power Systems and Electrical Technology (PSET) (pp. 607-612). IEEE.
[13] Yuan, H., Ye, H., Chen, Y., & Deng, W. (2022). Research on the optimal configuration of photovoltaic and energy storage in rural microgrid. Energy Reports, 8, 1285-1293.
[14] Sayed, K., Abo-Khalil, A. G., & S. Alghamdi, A. (2019). Optimum resilient operation and control DC microgrid based electric vehicles charging station powered by renewable energy sources. Energies, 12(22), 4240.
[15] Zhou, H., Lu, F., & Liu, Y. (2023). Coordination control for output voltage of optical-storage independent microgrid based on adaptive optimisation. International Journal of Powertrains, 12(4), 299-310.
[16] Ku, T. T., & Li, C. S. (2021). Implementation of battery energy storage system for an island microgrid with high PV penetration. IEEE Transactions on Industry Applications, 57(4), 3416-3424.
[17] Gao, K., Wang, T., Han, C., Xie, J., Ma, Y., & Peng, R. (2021). A review of optimization of microgrid operation. Energies, 14(10), 2842.
[18] Mao, W., Dai, N., & Li, H. (2019). Economic Dispatch of Microgrid Considering Fuzzy Control Based Storage Battery Charging and Discharging. Journal of Electrical Systems, 15(3).
[19] Yandong, L., Yiwen, H., Nan, C., Jingyue, W. A. N. G., Xinming, S. H. A. O., Zhongchen, P. E. I., & Chuang, L. I. U. (2022). Study on power optimization method and coordinated control strategy of optical storage microgrid. Journal of Electrical Engineering, 17(1), 22-30.
[20] Wu, J., Xu, A., Peng, Y., Zhang, X., Li, Z., & Feng, Y. (2023, September). Research on the operation control strategy of optical storage and DC microgrid. In Journal of Physics: Conference Series (Vol. 2592, No. 1, p. 012088). IOP Publishing.
[21] J iaqian Fu, Yuying Sun, Yunhe Li, Wei Wang, Wenzhe Wei, Jinyang Ren... & Haoran Di. (2025). An investigation of photovoltaic power forecasting in buildings considering shadow effects: Modeling approach and SHAP analysis. Renewable Energy,245,122821-122821.

[22] Kuo Yang, Yanjie Cai & Jinrun Cheng. (2025). A deep learning model based on multi-attention mechanism and gated recurrent unit network for photovoltaic power forecasting. Computers and Electrical Engineering,123(PD),110250-110250.